AE-434
UDC 539.2/.3

AE-434

Influence of Elastic Anisotropy on Extended Dislocation Nodes

B. Pettersson

AKTIEBOLAGET ATOMENERGI
STUDSVIK, NYKÖPING, SWEDEN 1971

INFLUENCE OF ELASTIC ANISOTROPY ON EXTENDED DISLOCATION NODES

B. Pettersson

ABSTRACT

The interaction forces between the partial dislocations forming an extended dislocation node are calculated using elasticity theory for anisotropic media. The calculations are carried out for nodes of screw, edge and mixed character in Ag, which has an anisotropy ratio A equal to 3, and in a hypothetic material with A = 1 and the same shear modulus as Ag. The results are compared with three previous theories using isotropic elasticity theory by Brown and Thölén, Siems and Jössang et al. As expected, in Ag the influence of anisotropy is of the same order as the uncertainty due to the dislocation core energy.

Printed and distributed October 1971

LIST OF CONTENTS

INTRODUCTION

As mentioned by Brown and Thölén [1] (1964) one weakness of their formula for calculating the SFE from extended dislocation nodes is that the formula is only valid for elastically isotropic media. The elastic properties of the material only appear through the shear modulus μ and Poisson's constant ν. In recent years, the theory of dislocations in elastically anisotropic media has been developed far enough to allow a calculation of the SFE in much the same way as done by Brown and Thölén, but with the use of the proper elastic constants c_{11}, c_{12} etc. This of course makes the calculations more complicated and it is not possible to give a simple analytic expression to be used together with quantities measured on the extended node. Instead these quantities must be used as input in a computer program evaluating the SFE. However, since the SFE might be of interest for a material close to a phase boundary, where the material can be highly anisotropic, the possibility of avoiding the approximation of isotropy is valuable.

THEORY

In order to clarify the aim of the following review of the basic theory we first look at the equilibrium condition for a node. The SFE acts as a surface energy and gives rise to a force on the partial dislocation which tends to shrink the node. This force is balanced by the elastic interaction between the partials. This interaction depends on the elastic constants of the medium and on the dislocation configuration. Since all parts of the node interact with each other the configuration dependence is quite complicated and simplifications must be made in order to render the evaluation of the elastic interaction force in an anisotropic medium manageable.

An expression for the elastic interaction force, the Peach-Koehler force, may be derived as follows (e.g. Hirth and Lothe [2]).

The force per unit length on a straight dislocation is

$$\frac{\bar{F}}{L} = (\bar{b} \cdot \bar{\sigma}) \times \bar{\tau} \qquad (1)$$

where $\bar{\tau}$ is the dislocation direction and $\bar{\sigma}$ the stress tensor.

We want an expression for the force in the glide plane normal to the dislocation. (The glide plane is the plane containing both the dislocation line and the Burgers vector.) Choose $\bar{m}$ so that

$$\bar{m} = \bar{n} \times \bar{\tau} \tag{2}$$

where $\bar{n}$ is the unit vector normal to the dislocation glide plane. Then

$$\frac{\bar{F}}{L} \cdot \bar{m} = (\bar{b} \cdot \bar{\sigma}) \times \bar{\tau} \cdot \bar{m} = (\bar{b} \cdot \bar{\sigma}) \cdot \bar{\tau} \times \bar{m} = (\bar{b} \cdot \bar{\sigma}) \cdot \bar{n}$$

where

$$(\bar{b} \cdot \bar{\sigma}) \cdot \bar{n} = b_i \sigma_{ij} n_j$$

(Through out this paper the Einstein convention is used, i.e. the repeated Roman indices implies summation.)

Thus

$$F = b_i \sigma_{ij} n_j \tag{3}$$

where F is the force per unit dislocation length in the glide plane and normal to the dislocation.

The present problem is to find the stress field $\bar{\sigma}$ from the three partial dislocations forming a node. $\bar{\sigma}$ from a straight dislocation may be found by solving a sextic equation (c.f. Stroh [3]). Using the formalism developed by Malén and Lothe [4], this problem is transferred to a standard eigenvalue problem. They introduce (c.f. Stroh [3]) vectors $\bar{A}$ and $\bar{L}$ with components A_k and $\tau_\ell L_{\ell k}$ and matrices ab with components

$$a_i c_{ijk\ell} b_\ell = (ab)_{jk} \tag{4}$$

where $\bar{a}$ and $\bar{b}$ is a pair of the vectors $\bar{m}$, $\bar{n}$ and $\bar{\tau}$ in eqn. (2). Using Hooke's law

$$\sigma_{op} = c_{opqs} \frac{\partial u_q}{\partial x_s} \tag{5}$$

where u_q is the displacement and expressing the stresses in functions φ_{ij} so that

$$\sigma_{ij} = (\mathrm{curl}\ \bar{\varphi})_{ij} = e_{ik\ell} \frac{\partial}{\partial x_k} \varphi_{\ell j} \tag{6}$$

they finally obtain

$$N \begin{pmatrix} \bar{A} \\ \bar{L} \end{pmatrix} = p \begin{pmatrix} \bar{A} \\ \bar{L} \end{pmatrix} \tag{7}$$

where

$$N = - \begin{pmatrix} (nn)^{-1} nm & (nn)^{-1} \\ mn(nn^{-1})nm - mm & mn(nn)^{-1} \end{pmatrix} \tag{8}$$

This is a standard eigenvalue problem with six eigenvalues p_α and six eigenvectors $(\bar{A}_\alpha, \bar{L}_\alpha)$ in pairs of complex conjugates.

From Malén and Lothe [4] we find the stress from a straight dislocation through the origin, in the $\bar{\tau}$-direction, expressed in the x-cordinates:

$$\sigma_{ij} = c_{ijk\ell} \frac{1}{2\pi i} \sum_{\alpha=1}^{6} A_{k\alpha} (\pm 1) L_{s\alpha} b_s \frac{m_\ell + p_\alpha n_\ell}{\bar{m} \cdot \bar{x} + p_\alpha \bar{n} \cdot \bar{x}} \tag{9}$$

where the eigenvectors are normalized.

From the stress in the plane $\bar{x} \cdot \bar{n} = 0$ at unit distance from the dislocation $(\bar{m} \cdot \bar{x} = 1)$ we obtain the stress factor Σ_{ij} (c.f. Brown [5])

$$\Sigma_{ij} = c_{ijk\ell} \frac{1}{2\pi i} \sum_{\alpha=1}^{6} A_{k\alpha} (\pm 1) L_{s\alpha} b_s (m_\ell + p_\alpha n_\ell) \tag{10}$$

The angular factor

$$\Phi_{ij} (\varphi) = \Sigma_{ij} (\varphi) + \frac{\partial^2 \Sigma_{ij} (\varphi)}{\partial \varphi^2} \tag{11}$$

where $\Sigma_{ij} (\varphi)$ is the stress factor for a straight dislocation in the direction specified by φ, can be used to evaluate the elastic field from a curved dislocation loop (Malén and Lothe [4])

$$\sigma_{ij} (\bar{r} = 0) = \frac{1}{2} \oint \Phi_{ij} (\varphi) \, r^{-1} \, d\varphi \tag{12}$$

r and φ are the polar coordinates for the dislocation element $d\varphi$ which is integrated over. The second derivative of $\Sigma_{ij} (\varphi)$ with respect to φ may easily be obtained from eqn. (10) (c.f. Malén and Lothe [4]).

Expression (12) is used in the present paper to find the stress from the three partials forming an extended node. It might be evaluated by calculating $\Phi_{ij} (\varphi)$ for several directions and using numerical integration.

In order to avoid this time-consuming treatment of the problem, we choose to expand $\Sigma_{ij}(\varphi)$ up to second order around a given direction.

$$\Sigma_{ij}(\varphi) = \Sigma_{ij}(0) + \varphi\,\Sigma'_{ij}(0) + \frac{\varphi^2}{2}\,\Sigma''_{ij}(0) + \ldots\ldots \tag{13}$$

The nodes in fcc materials are situated on the (111)-planes which possess 3-fold symmetry. If the series expansion is carried out for φ up to $\frac{\pi}{3}$, we cover the whole node plane by only one calculation of Σ_{ij} and its derivatives. Realizing that

$$\Sigma_{ij}(\varphi) = (-1)^{i+j}\,\Sigma_{ij}(\varphi + \pi) \tag{14}$$

we can restrict ourselves to expand Σ_{ij} up to $\varphi = \frac{\pi}{6}$.

Instead of finding the derivatives of Σ_{ij} by direct differentiation of expression (10), let us carry out some simplifications. Inserting $\bar{\xi} = \bar{n}x\bar{\tau} + p\bar{n}$ into eq. (2.9) in the paper of Malén and Lothe [4] gives

$$\tau_\ell L_{\ell j} = -n_i c_{ijk\ell} A_k (p n_\ell + m_\ell) \tag{15}$$

Using $c_{ijk\ell} = c_{jik\ell}$ and $\tau_\ell L_{\ell j} = L_j$ (by definition) and exchanging the positions of i and j, eq. (15) becomes:

$$L_i = -n_j c_{ijk\ell} A_k (m_\ell + p n_\ell) \tag{16}$$

Multiplying both sides of eq. (10) by n_j we obtain

$$\Sigma_{ij} n_j = c_{ijk\ell}\,\frac{1}{2\pi i}\sum_{\alpha=1}^{6} A_{k\alpha}\,(\pm 1) L_{s\alpha} b_s (m_\ell + p_\alpha n_\ell) n_j \tag{17}$$

Hence, by eqs. (16) and (17)

$$\Sigma_i = \Sigma_{ij} n_j = \frac{1}{2\pi i}\sum_{\alpha=1}^{6} (\mp 1) L_{s\alpha} L_{i\alpha} b_s \tag{18}$$

Define $b_s \Lambda_{si} = \Sigma_i$, giving

$$\Lambda_{si} = \frac{1}{2\pi i}\sum_{\alpha=1}^{6} (\mp 1) L_{s\alpha} L_{i\alpha} \tag{19}$$

Since $\frac{\partial n_j}{\partial \varphi} = 0$ and b_s is a constant we obtain the derivatives of $\Sigma_{ij} n_j$ by differentiation of the rather short expression (19):

$$\Lambda'_{si} = \frac{1}{2\pi i} \sum_{\alpha=1}^{6} (\mp 1)(L_{s\alpha} L'_{i\alpha} + L'_{s\alpha} L_{i\alpha}) \tag{20}$$

$$\Lambda''_{si} = \frac{1}{2\pi i} \sum_{\alpha=1}^{6} (\mp 1)(L_{s\alpha} L''_{s\alpha} + L''_{s\alpha} L_{i\alpha} + 2L'_{s\alpha} L'_{i\alpha}) \tag{21}$$

The derivatives of $\bar{L}$ are expressed in eqs. (3.8) and (3.11) in ref. [4].

The functions Λ_{si} are explicitly related to the stress factors Σ_{ij} through

$$\Sigma_{ij} n_j = b_s \Lambda_{si} \tag{22}$$

Multiplying eq. (12) with n_j and using eqs. (11), (13) and (22) we obtain the stress field

$$2\sigma_{ij} n_j = b_s \{ [\Lambda_{si}(0) + \Lambda''_{si}(0)] \oint r^{-1} d\varphi + \Lambda'_{si}(0) \oint \varphi r^{-1} d\varphi + \\ + \frac{1}{2} \Lambda''_{si}(0) \oint \varphi^2 r^{-1} d\varphi \} \ldots . \tag{23}$$

Combined with eq. (3) this gives us the force per unit dislocation length in the glide plane and normal to the dislocation. However, eq. (23) is insoluble at the points in which we are interested, namely on the partial dislocation itself. The reason is that r, the distance between the field point and the source point, approaches zero as we perform the integration if the field point and the source point are situated on the same partial. (The field point is the point where we wish to calculate the stresses, the source point is the position of the dislocation segment giving rise to the stresses.) The field point must be moved away from the partial, and, using Brown's [6] definition of the self stress, the force per unit length on any dislocation element due to the configuration of which it is a part is

$$F(\bar{r}) = \frac{1}{2} [F(\bar{r} + \bar{\varepsilon}) + F(\bar{r} - \bar{\varepsilon})] \tag{24}$$

where $\bar{\varepsilon}$ is a vector of length approximately equal to the inner cut-off radius and normal to the dislocation line. $|\varepsilon|$ is in the present work chosen to be 5 Å.

The dependence of r^{-1} upon φ is determined by the specific dislocation configuration for which the calculations are carried out. In the pre-

sent work three different shapes of the partials at the node are tested, a hyperbolic, a parabolic and a circular shape. The latter two second degree curves are smoothly joined to straight lines describing the partials forming the node legs. Since the parabolic assumption is found to give the most evenly distributed force on the partials at the node, the partials in the present work are assumed to consist of two infinite straight lines joined to a part of a parabola. The vertex of the parabola is symmetrically placed with respect to the two straight segments of the partial. Thus, the appearance of a node is fully determined by:

1) The parameters of the three parabolas at the node
2) The position of the foci of the parabolas relative to each other
3) The angles between the node legs
4) The orientation of the node in the lattice

Let us summarize the procedure to find the SFE from a stacking fault node, photographed in an electron microscope. The node must be observed in three different orientations each with one of the node legs out of contrast. (A node leg does not give any contrast when its Burgers vector is contained in the reflecting plane.) Using standard electron diffraction technique we are then able to fully determine the node plane, the orientation of the node, the angle between the node plane and the electron beam, and the Burgers vectors of the partials forming the node.

The eigenvalue problem (eq. (7)) is then solved and the Λ-factors are determined for the node plane. This is done using a slightly modified version of a computer programme written by K. Malén [7]. The Λ-matrix is then used together with the measured quantities of the node (points 1 - 4 above) as input in another computer programme which solves eq. (23) and calculates the force per unit length on a dislocation by eq. (3). This programme makes use of eq. (24) and the symmetry of a (111)-plane in fcc. (See ref. [13]).

CALCULATIONS

The series expansion of the stress factors Σ_{ij} is of interest not only for the present work, but is of use in many problems involving dislocation interactions. Fig. 1 shows the degree of validity of the expansion of Λ_{ij} around the $[10\bar{1}]$-direction on the $[1\bar{1}1]$-plane in Ag. Λ_{ij} is related to the stress factors through eq. (22). The numbers in the figures are given in 10^{11} dyn/cm^2.

The expansion gives almost exact values for $\varphi = 10^{\circ}$. When $\varphi = 20^{\circ}$

the greatest absolute deviation is $\sim 0.015 \cdot 10^{11}$ dyn/cm^2 for Λ_{22}. The greatest relative deviation, 12 per cent, is shown by Λ_{12}. This deviation has risen to more than 50 per cent when $\varphi = 30^o$.

In the present work the SFE is calculated from node measurements in an anisotropic material. The material chosen is Ag, which has an anisotropy ratio A = 3.0. In order to compare the anisotropic calculations with an isotropic average, we have constructed an elasticity matrix for Ag with A = 1.05. (A = 1, the fully isotropic value, can not be used owing to limitations in the computer programme.)

The following relations are valid for an isotropic material:

$$\mu = c_{44} = \frac{1}{2}(c_{11} - c_{12}) \tag{25}$$

$$\lambda = c_{12} \tag{26}$$

where μ is the shear modulus and λ the Lamé constant. The Voigt mean values of μ and λ for Ag are $3.38 \cdot 10^{11}$ dyn/cm^2 and $8.11 \cdot 10^{11}$ dyn/cm^2 respectively (ref. 2). From this $c_{11} = \lambda + 2\mu = 14.87$. We put $c_{44} = \mu$ and determine c_{12} so as to give A = 1.05 which gives

$$c_{11} = 14.87 \cdot 10^{11} \text{ dyn/cm}^2$$

$$c_{12} = 8.43 \cdot 10^{11} \text{ dyn/cm}^2$$

$$c_{44} = 3.38 \cdot 10^{11} \text{ dyn/cm}^2$$

Let us call this material IS (isotropic silver). For Ag the elastic constants are (ref. 2):

$$c_{11} = 12.40 \cdot 10^{11} \text{ dyn/cm}^2$$

$$c_{12} = 9.34 \cdot 10^{11} \text{ dyn/cm}^2$$

$$c_{44} = 4.61 \cdot 10^{11} \text{ dyn/cm}^2$$

For a given stacking fault node, equations using isotropic elasticity theory will give the same SFE whether the node is in IS or in Ag. In order to extract the influence of anisotropy on the SFE value one obtains from measurements of a certain node, we have assumed a SFE = 21 erg/cm^2 in both Ag and IS, calculated the node appearance in Ag and IS, and compared the results. This is done for screw ($\alpha = 0$), edge ($\alpha = \pi/2$) and

mixed ($\alpha = \pi/4$) nodes. (α is the angle between a node leg and its Burgers vector.) The force per unit length is calculated for six points on one partial, situated as shown in fig. 2 ($v = 1/7 \cdot (2\pi - 4u)$).

The result is shown in table 1 - 6. A, D and β in table a) are parameters specifying the node appearance. A gives the curvature of the parabolic segments of the partials (see fig. 2) and D and β give the relative positions of the three partials (see fig. 3). The indices I, II and III specify to which partial a certain parameter belongs. As shown in fig. 2 the partial dislocations are called I, II and III. The field points are always situated on partial III. Table a) also gives the mean value of the SFE for the six field points together with the standard deviation. The separation s of the partials and the radius of the inscribed circle found in the calculations are also shown in table a). Table b) gives not only the total force F_T in each field point but also the contributions F_I, F_{II} and F_{III} from each partial. F_{III} is generally called the self force.

Table 7 compares the values of the SFE in the present work with the values found for the same nodes with three previous formulas for SFE-determination. Brown and Thölén [1], Siems [8] and Jössang et al. [9].

Calculations have also been carried out for two real nodes in Ag, shown in fig. 4. Since the plane perpendicular to the electron beam was (101), the nodes are seen projected on that plane. Node A is a rather symmetric* node deviating $\sim 10^{\circ}$ from pure screw character, while node B is asymmetric with the out of contrast leg having pure screw character. The results of the calculations are shown in table 8 - 13. The field points 1 - 4 in those tables correspond to the points 2 - 5 in fig. 2. The outer points have been omitted since the force at these points depends strongly on the separation of the partials. Hence, contrast displacement from the true dislocation position will be important.

ERROR DISCUSSION

Let us estimate the error in the calculations introduced by using a series expansion of Λ_{ij} over as much as 30°. Using eqs. (3) and (23) we obtain:

$$F = b_i b_j R(\Lambda_{ij}, r, \varphi)$$

---

* The word "symmetric" refers to the node appearance. All nodes in this report are symmetric in the sense that the node legs are of the same character.

where R is a function of Λ_{ij}, and the derivatives of Λ_{ij}, r and φ. However, the Burgers vectors must be expressed in the same system as Λ_{ij}, i. e. the $(\bar{m}, \bar{n}, \bar{\tau})$-system, and they are situated in the $(\bar{m}, \bar{\tau})$-plane (the glide plane). Hence b_2 equals zero and the only Λ-factors contributing to F are Λ_{11}, Λ_{13}, Λ_{31} and Λ_{33}. With $\varphi = 30^{\circ}$ the deviation for Λ_{13} is 23 per cent of the true value, but the total effect of the series expansion will be considerably less.

The relative error introduced by integrating the series expansion instead of using the true values of Λ_{ij} is:

$$p_{ij} = \frac{\int \Lambda_{ij}(\varphi)\, d\varphi - \int [\Lambda_{ij}(\varphi) - \nu(\varphi)] d\varphi}{\int \Lambda_{ij}(\varphi)\, d\varphi}$$

where $\nu(\varphi)$ are the deviation between $\Lambda_{ij}(\varphi)$ and the series expansion. Thus p is found by dividing the area under the difference curve by that under the $\Lambda_{ij}(\varphi)$ curve. This gives $p_{13} \sim 11$ per cent, $p_{11} < 1$ per cent and $p_{33} < < 1$ per cent. If these percentual errors are weighted with the absolute values of the relevant Λ_{ij}, the total error in F will be about 2 per cent.

The main weakness in the calculations is the assumption of a parabolic form of the partial dislocations. This prevents the calculations from being carried out for a dislocation in its proper equilibrium state. The difference between the values obtained in various field points is a measure of the validity of the parabolic form. As can be seen from tables 1 - 6, the greatest error is introduced for the edge nodes, while the parabolic form is a rather good assumption for screw nodes. However, a programme using the parabolic form is found to be superior to programmes using either a circular or a hyperbolic form.

The calculations are based on elasticity theory and the dislocations are assumed to have zero width. No attention is paid to core energies which may amount to some tenth of the total dislocation energy. However, by varying the core radius ϵ in eqn. (24) we can achieve some correction for the core energy. Using ϵ equal to 3 Å instead of 5 Å changes the values obtained for a edge node in IS by up to 7 per cent. The sign and amount of the change differs for the various field points.

If we choose ϵ to be smaller than is justified from the point of view of linear elasticity theory, we obtain a contribution to $F(\bar{r})$ from the core region. The magnitude of this contribution depends on the choice of ϵ. The value $\epsilon = 5$ Å used in this report is chosen from two criteria:

1) ϵ must be smaller than the true core radius in order to give some correction for the core energy, and, 2) ϵ must not be too small, since $F(\bar{r} + \bar{\epsilon})$ and $F(\bar{r} - \bar{\epsilon})$ increase with decreasing ϵ and the formula (24) may also become dependent on the numerical exactitude of the computer.

The assumption of zero dislocation width implies that the calculations is spoiled as the separation of the dislocations becomes comparable with the core radius.

DISCUSSION

From tables 1 - 6 we are able to draw some conclusions on the influence of anisotropy on the node appearance. Comparing Ag with IS, the radius of curvature R (R = 2A) for the partial dislocations at the node are almost unchanged for a node of screw or mixed character. However, for a node of pure edge character, R decreases by about 10 per cent when the anisotropy ratio is increased from 1.05 to 3.02. The radius of a circle inscribed in the node, w, is more seriously affected. For a screw node, w decreases by 21 per cent, for an edge node by 9 per cent. As can be seen from the values of β, a mixed node with $\alpha = 45^{\circ}$ becomes only slightly more asymmetric when the anisotropy ratio increases.

It is interesting to compare the various contributions to the force from the three partials. The contribution to the force at the vertex of the parabola from the self stress is for a screw node in IS 70 per cent and in Ag 80 per cent, for an edge node in IS it is 35 per cent, in Ag 15 per cent, for a mixed node in IS it is 60 per cent, in Ag 62 per cent. Hence, in Ag an isotropic approximation tends to overestimate the self-stress for edge nodes but to slightly underestimate it for screw nodes. For the edge node in Ag we obtain negative self-stress in four points, i.e. the self-stress actually tries to reduce the size of the node at these points. However, such a result is expected, since an infinite straight Shockley partial of edge character in the noble metals Cu, Ag and Au has negative line tension. (For Cu c.f. Clarebrough and Head [10] and Pettersson and Malén [14], for Ag and Au c.f. ref. [14].) The bent shape of the partials forming a node causes the negative value of the selfstress to occur at points where the dislocation is not of pure edge character.

Table 7 compares the present theory with previous theories. A comparison between the theory of Brown and Thölén and that of Siems has been made by Ruff [11]. The theories do agree well for screw nodes, while for a given shape of an edge node, the theory of Siems gives much

lower SFE values than that of Brown and Thölén. This is also evident from table 7.

Before making any comparison between the present and previous theories, it should be pointed out that the present theory is believed to give higher accuracy for the SFE in Ag than in IS. IS is a constructed material and as such it implies an assumption.

The values for SFE for a screw node in Ag obtained by all three isotropic theories are significantly higher than the values from the present theory. However, even in IS the same disagreement is apparent when using the radius of curvature formulas or the Jössang et al. formula. This disagreement can not be explained by elastic anisotropy, but must depend on the mathematical treatment of the entire problem. Jössang et al. assumes the node to consist of straight dislocation parts and this assumption together with the uncertainty in the core energy, are believed to be the main cause of the deviations between the result of their theory and the result from the present report. However, the deviation for a screw node is increased as anisotropy is taken into account. This is due to shrinkage of the node as the anisotropy ratio is increased. The same effect also causes the difference between the values of the SFE for an edge node, obtained by the Jössang et al. method.

Brown and Thölén do not assume any particular shape of the partial dislocations, but, using an iterative process, they find the shape which minimizes the total stresses at various points on the partials. The stresses are said to be minimized if they are less than 1 per cent of the stresses caused by the stacking fault. As can be seen in tables 1 - 6 the same accuracy is obtained for screw nodes in the present report. while the accuracy for mixed and edge nodes is reduced by fixing the partial to a parabolic shape. This implies that the partials surrounding a node of screw character, are properly described by the parabolic assumption, and the parameters A and w in table 1a and 2a are accurate.

However, although the same cut-off radius is used in all formulas except the one of Jössang et al. we still have an unspecified energy contribution from the core in the different formulas. This contribution probably amounts to about ten per cent of the value of the force on the partial. Keeping the above-mentioned uncertainties in mind, the following comparison between the present theory and the theory of Brown and Thölén may be made. Starting with the formula using R in the isotropic material, we find that the present theory does not show the same strong

dependence of R on the node character, specified by α. The present theory in fact gives a higher value to R for a mixed node than for a screw node, while the Brown and Thölén formula gives a decreasing R as α increases. The same discrepancy between the theories is found for the inscribed radius w. Increasing anisotropy tends to raise the differences in w. This is probably due to overestimation of the forces from the other partials of the screw node, when performing isotropic calculations. For the edge node, the negative self-stress causes the node to shrink more than in the isotropic case. The formula of Brown and Thölén using R seems to be slightly less dependent on anisotropy than the formula using w.

The theory of Siems (see also Siems et al. [12]) minimizes the total energy of the node in order to find the equilibrium shape. However, these authors only take into account the interaction energy between those parts of the partials which comprise the same node leg, i.e. they neglect, for example, the force 10.87 dyn/cm and partly the force 7.64 dyn/cm at point 4 in table 6b. This causes their theory to yield wrong values for the radius of curvature, and the error is increased as the deviation of the node character from pure screw is increased. The values obtained by using w in the theory of Siems are not so seriously affected by neglecting part of the interaction energy, however, and we conclude that this parameter is superior to R when using the theory of Siems.

The real node A (fig. 4) in Ag appears at first glance to be very symmetric. The values of the forces at various points, shown in tables 8 - 10, also confirm this impression. From these tables we see that the size of the node seems to be almost entirely determined by the self-stress. However, since this node deviates only 10° from pure screw character, a comparison with tables 2 and 6 shows that the force contribution from partials 1 and 2 are too low in tables 8 - 10. The contrast from the partials have made the node appear larger than its true size. Point 1 on partial 2 and point 3 on partial 3 both show high values of the force, indicating that the parabola approximation cannot properly represent a true node. The mean value of the SFE achieved from the present theory is 15.2 erg/cm^2. The Brown and Thölén formula gives 18.0 erg/cm^2 using the radius of curvature R and 14.4 erg/cm^2 using the inscribed radius w. As for the constructed screw nodes, an isotropic theory using R gives too high a value of SFE. The number 14.4 is rather close to 15.2, but the inscribed radius is overestimated owing to the false node contrast.

Node B (fig. 4) has the node leg consisting of partials 2 and 3 tied at point P, rendering the node rather asymmetric. Tables 11 - 13 show how this affects the forces at various points on the node. Although partial 1 is less curved than partial 2, it is affected by stronger forces. The force from partial 2 on partial 1 (F_1 in table 11) is enhanced owing to the relatively sharp curvature of partial 2. Since partial 1 is the only partial in node B of pure screw character at the vertex of the parabola it has also relatively high self-stress. The mean value of the SFE from tables 11 - 13 is 22.8 erg/cm^2. Brown and Thölén give 26.6 erg/cm^2 using R and 21.2 using w.

The SFE for nodes A and B obtained from the present anisotropic calculations differ as much as the values obtained by the Brown and Thölén formulas. This indicates that the large deviations from the mean values of the SFE, shown by certain nodes when using the node method, are not caused by the isotropic approximation in the equations used. Forces from the specimen surfaces and from surrounding dislocations almost entirely determine these deviations.

SUMMARY

For a material with a certain SFE, the present theory does not predict such a strong dependence of the SF node size on the node character as previous theories. In fact, nodes of mixed character are found to be bigger than screw nodes even in a material with an anisotropy ratio A = 1.05. This result is more pronounced when A is increased to 3.

The error introduced by using isotropic theories to calculate the SFE in Ag is overshadowed by disturbances from the specimen surfaces and from surrounding dislocations. However, certain effects of anisotropy on the node appearance are found, and these effects may become important when measuring the SFE in an alloy system close to a phase limit where A may be high.

ACKNOWLEDGEMENT

The author wishes to thank Dr. K. Malén for many valuable ideas and helpful discussions.

REFERENCES

1. BROWN, L. M. and THÖLÉN, A. R.,
Shape of three-fold extended nodes.
Disc. Faraday Soc. 38 (1964) p. 35.

2. HIRTH, J. P. and LOTHE, J.,
Theory of dislocations. McGraw-Hill (1968).

3. STROH, A. N.,
Steady state problems in anisotropic elasticity.
J. Math. Phys. 41 (1962) p. 77.

4. MALÉN, K. and LOTHE, J.,
Explicit expressions for dislocation derivatives.
Phys. Stat. Sol. 39 (1970) p. 287.

5. BROWN, L. M.,
A proof of Lothe´s theorem.
Phil. Mag. 15 (1967) p. 363.

6. BROWN, L. M.,
The self-stress of dislocations and the shape of extended nodes.
Phil. Mag. 10 (1964) p. 441.

7. MALÉN, K.,
1968. AB Atomenergi, Sweden.
(Internal report no. AE-FMF-53).

8. SIEMS, R.,
Shape of extended nodes.
Disc. Faraday Soc. 38 (1964) p. 42.

9. JØSSANG, T. et al.,
On the determination of stacking fault energies from extended dislocation node measurements.
Acta Met. 13 (1965) p. 279.

10. CLAREBROUGH, L. M. and HEAD, A. K.,
Unstable directions of Shockley partial dislocations.
Phys. Stat. Sol. 33 (1969) p. 431.

11. RUFF, A. W. Jr.,
Measurement of stacking fault energy from dislocation interactions.
Met. Transactions 1 (1970) p. 2391.

12. SIEMS, R., DELAVIGNETTE, R. and AMELINCKX, S.,
Die direkte Messung von Stapelfehlerenergien.
Z. Physik 165 (1961) p. 502.

13. PETTERSSON, B.,
1971. AB Atomenergi, Sweden.
(Internal report no AE-MF-218).

14. PETTERSSON, B. and MALÉN, K.,
Dislocation line tensions in the noble metals, the alkali metals and β-brass.
1971 (AE-426).

Table 1. Screw node in isotropic Ag

a)*

A_{I-III}	D_{I-II}	β_I	β_{II}	SFE	S	w
180	470	2.618	3.665	20.9±0.2	55	92

b)**

Point	F_I	F_{II}	F_{III}	F_T
1	6.87	1.46	12.60	20.93
2	4.99	1.93	14.14	21.06
3	3.58	2.61	14.61	20.80
4	2.61	3.58	14.39	20.58
5	1.93	4.99	14.08	21.00
6	1.46	6.87	12.52	20.85

Table 2. Screw node in Ag

a)

A_{I-III}	D_{I-II}	β_I	β_{II}	SFE	S	w
177.5	433	2.618	3.665	20.7±0.2	23	72.5

b)

Point	F_I	F_{II}	F_{III}	F_T
1	5.15	0.93	14.37	20.45
2	3.46	1.26	16.20	20.92
3	2.46	1.76	16.51	20.73
4	1.76	2.48	16.60	20.84
5	1.25	3.48	16.10	20.83
6	0.93	5.21	14.26	20.40

* A, D, S and w in Angstrom, β in radians, SFE in erg/cm^2

** F in dyn/cm

Table 3. Edge node in isotropic Ag

a)

A_{I-III}	D_{I-II}	β_I	β_{II}	SFE	S	w
155	430	2.618	3.665	20.9±0.9	71	93

b)

Point	F_I	F_{II}	F_{III}	F_T
1	14.50	3.32	4.00	21.82
2	11.20	4.29	4.21	19.70
3	7.95	5.71	7.48	21.14
4	5.71	7.95	7.43	21.09
5	4.29	11.20	4.23	19.72
6	3.32	14.50	4.03	21.85

Table 4. Edge node in Ag

a)

A_{I-III}	D_{I-II}	β_I	β_{II}	SFE	S	w
140	390	2.618	3.665	20.8±1.7	66	85

b)

Point	F_I	F_{II}	F_{III}	F_T
1	18.88	4.25	-1.33	21.80
2	14.79	5.51	-1.75	18.55
3	10.88	7.64	3.40	21.92
4	7.64	10.87	3.18	21.69
5	5.51	14.77	-1.68	18.60
6	4.25	18.88	-1.20	21.93

Table 5. Mixed node in isotropic Ag ($\alpha = \pi/4$)

a)

A_{I-III}	D_{I-II}	β_I	β_{II}	SFE	S	w
210	555	2.524	3.5712	20.9±0.4	68	112

b)

Point	F_I	F_{II}	F_{III}	F_T
1	6.44	3.20	11.29	20.93
2	3.44	4.13	12.83	20.40
3	2.15	5.52	12.70	20.37
4	1.43	7.29	12.74	21.46
5	1.08	10.02	10.04	21.14
6	0.83	13.00	7.10	20.93

Table 6. Mixed node in Ag ($\alpha = \pi/4$)

a)

A_{I-III}	D_{I-II}	β_I	β_{II}	SFE	S	w
210	550	2.498	3.545	20.7±0.9	61	112

b)

Point	F_I	F_{II}	F_{III}	F_T
1	3.50	4.03	12.56	20.09
2	1.25	5.33	14.10	20.68
3	0.42	6.49	13.45	20.36
4	0.01	9.21	13.25	22.47
5	0.01	10.95	9.24	20.20
6	0.00	15.00	5.29	20.29

Table 7.

α	Material	Present work	Brown & Thölén		Siems		Jössang et al.
			$\gamma(\frac{1}{R})$	$\gamma(\frac{1}{w})$	$\gamma(\frac{1}{R})$	$\gamma(\frac{1}{w})$	
0	IS	20.9	25.7	21.5	23.7	20.8	24.0
	Ag	20.7	25.8	27.3	24.0	25.8	29.5
45	IS	20.9	17.5	19.3	14.3	16.4	14.0
	Ag	20.7	17.5	19.3	14.3	16.4	14.0
90	IS	20.9	17.0	24.2	9.5	17.3	15.0
	Ag	20.8	18.3	26.1	10.9	18.8	16.0

Table 8. Partial 1, node A

a)

A	D_I	D_{II}	β_I	β_{II}	SFE
257	641	715	2.593	3.615	14.1

b)

Point	F_I	F_{II}	F_{III}	F_T
1	2.33	0.13	12.14	14.60
2	1.91	0.15	12.35	14.41
3	1.61	0.15	12.21	13.97
4	1.23	0.12	12.02	13.37

Table 9. Partial 2, node A

a)

A	D_I	D_{II}	β_I	β_{II}	SFE
223	672	641	2.460	3.628	15.6

b)

Point	F_I	F_{II}	F_{III}	F_T
1	1.86	0.20	15.32	17.38
2	1.60	0.23	13.44	15.27
3	1.35	0.23	13.62	15.20
4	1.10	0.22	13.24	14.56

Table 10. Partial 3, node A

a)

A	D_I	D_{II}	β_I	β_{II}	SFE
257	715	672	2.545	3.505	15.4

b)

Point	F_I	F_{II}	F_{III}	F_T
1	2.26	0.23	11.97	14.43
2	1.90	0.28	12.60	14.78
3	1.43	0.32	16.85	18.60
4	1.13	0.20	12.27	13.60

Table 11. Partial 1, node B

a)

A	D_I	D_{II}	β_I	β_{II}	SFE
151	387	482	2.575	3.62	27.9

b)

Point	F_I	F_{II}	F_{III}	F_T
1	8.70	0.60	18.38	27.68
2	7.50	0.70	19.12	27.32
3	5.82	0.85	19.28	25.95
4	4.66	0.93	25.25	30.84

Table 12. Partial 2, node B

a)

A	D_I	D_{II}	β_I	β_{II}	SFE
126	429	387	2.505	3.75	24.4

b)

Point	F_I	F_{II}	F_{III}	F_T
1	4.26	0.70	15.24	20.20
2	3.43	1.00	21.74	26.17
3	2.73	1.28	22.38	26.39
4	2.13	1.63	21.12	24.88

Table 13. Partial 3, node B

a)

A	D_I	D_{II}	β_I	β_{II}	SFE
185	482	429	2.690	3.61	16.2

b)

Point	F_I	F_{II}	F_{III}	F_T
1	1.46	-0.25	14.92	16.13
2	1.36	-0.42	15.00	15.94
3	1.20	-0.27	14.74	15.67
4	1.05	1.07	14.75	16.87

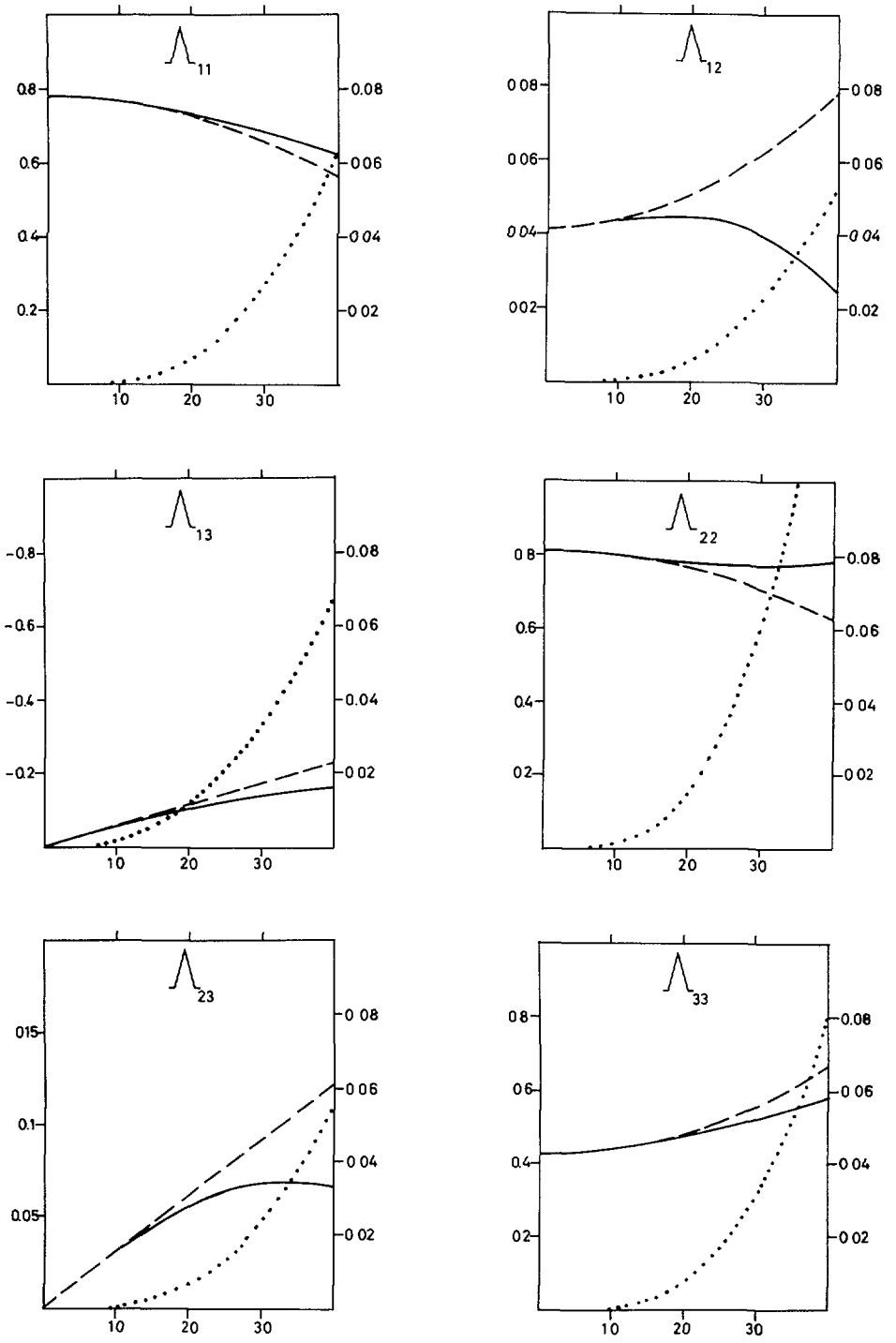

Fig. 1. Variation of Λ_{ij} on the $(1\bar{1}1)$ plane in Ag in 10^{11} dyn/cm^2. The horisontal axis shows the angle of deviation from the $[10\bar{1}]$ direction.

——— True value (numbers on the left vertical axis)

----- Value from series expansion (numbers on the left vertical axis)

····· Difference (numbers on the right vertical axis)

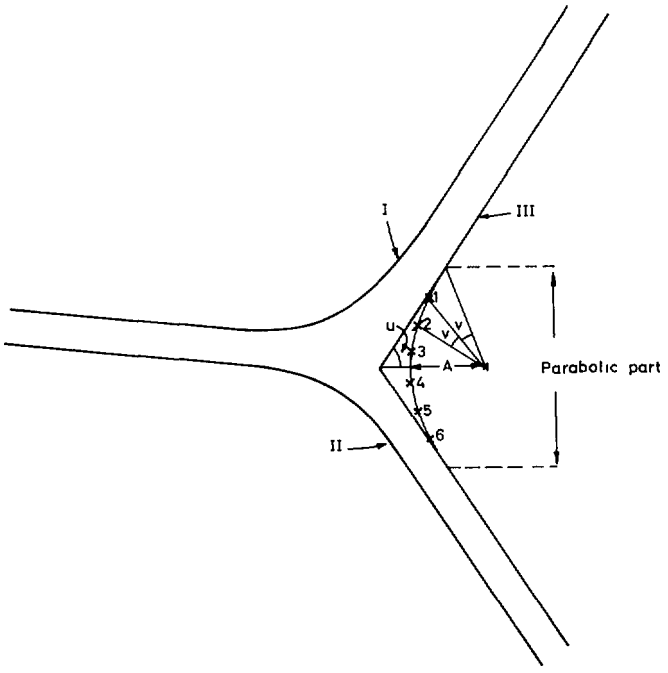

Fig. 2. Position of points of calculations. A and u specify the shape of the partial dislocation.

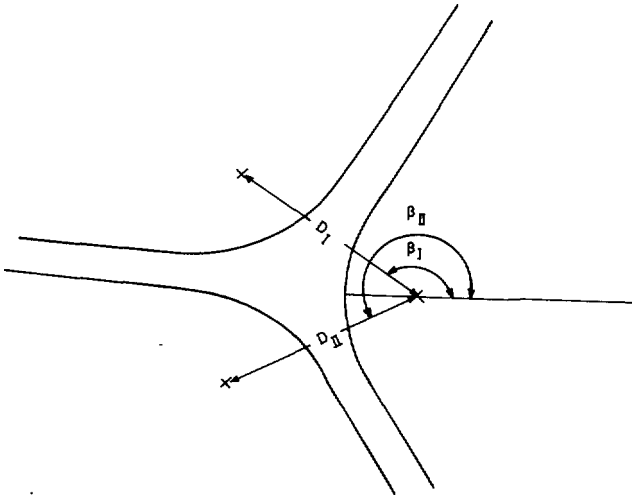

Fig. 3. D and β specify relative position of the partial dislocations.

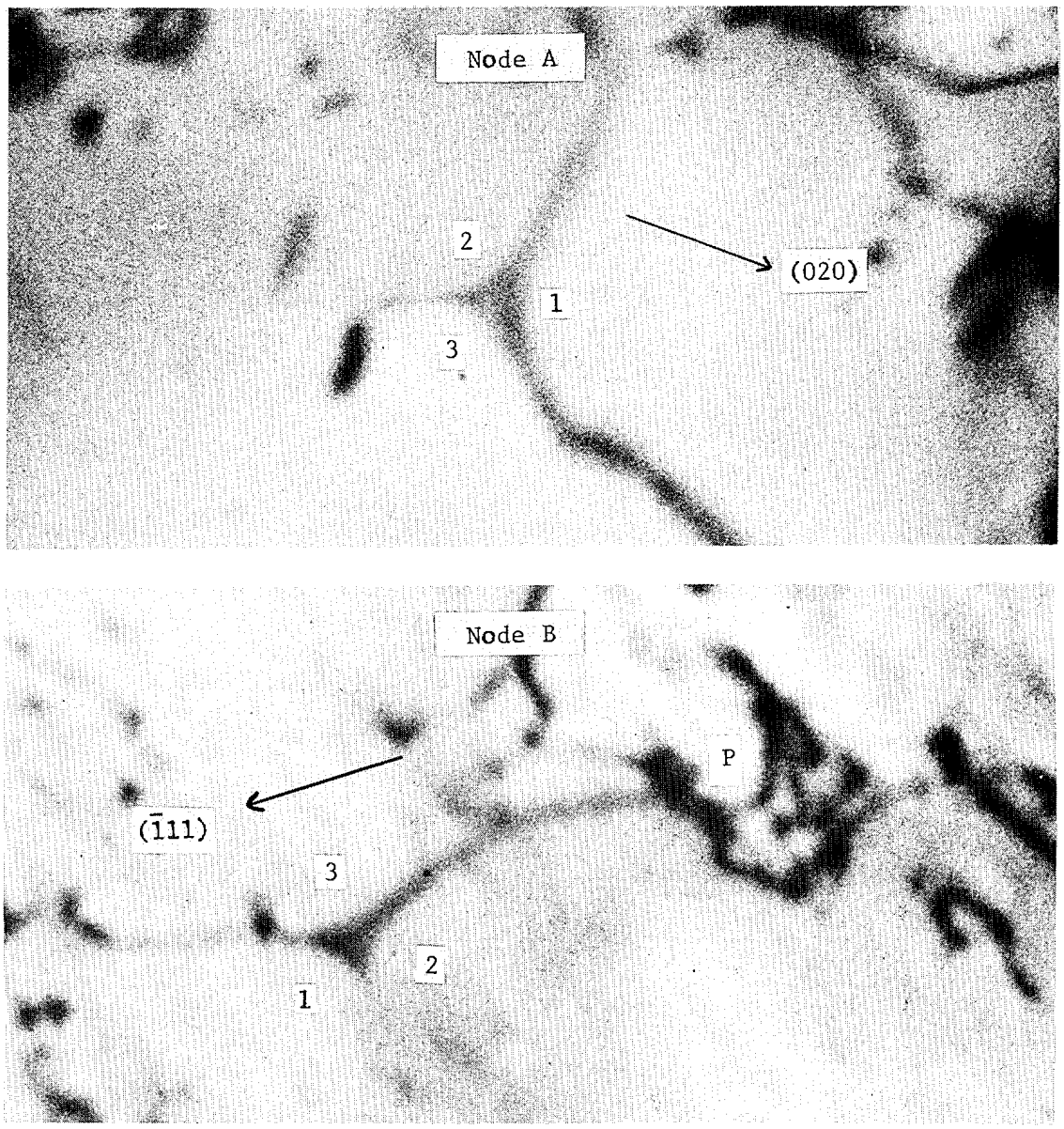

Fig. 4. Extended nodes in Ag.
Magnification: 285 000

LIST OF PUBLISHED AE-REPORTS

1–360 (See back cover earlier reports.)

361. A half-life measurement of the 343.4 keV level in ^{175}Lu. By M. Höjeberg and S. G. Malmskog. 1969. 10 p. Sw. cr. 10:–.

362. The application of thermoluminescence dosimeters to studies of released activity distributions. By B-I. Rudén. 1969. 36 p. Sw. cr. 10:–.

363 Transition rates in ^{161}Dy. By V. Berg and S. G. Malmskog. 1969. 32 p. Sw. cr. 10:–.

364. Control rod reactivity measurements in the Ågesta reactor with the pulsed neutron method. By K. Björeus. 1969. 44 p. Sw. cr. 10:–.

365. On phonons in simple metals II. Calculated dispersion curves in aluminium. By R. Johnson and A. Westin. 1969. 124 p. Sw. cr. 10:–.

366. Neutron elastic scattering cross sections. Experimental data and optical model cross section calculations. A compilation of neutron data from the Studsvik neutron physics laboratory. By B. Holmqvist and T. Wiedling. 1969. 212 p. Sw. cr. 10:–.

367. Gamma radiation from fission fragments. Experimental apparatus – mass spectrum resolution. By J. Higbie. 1969. 50 p. Sw. cr. 10:–.

368. Scandinavian radiation chemistry meeting, Studsvik and Stockholm, September 17–19, 1969. By H. Christensen. 1969. 34.p. Sw. cr. 10:–.

369. Report on the personnel dosimetry at AB Atomenergi during 1968. By J. Carlsson and T. Wahlberg. 1969 10 p. Sw. cr. 10:–.

370. Absolute transition rates in ^{188}Ir. By S. G. Malmskog and V. Berg. 1969. 16 p. Sw. cr. 10:–.

371. Transition probabilities in the 1/2+(631) Band in ^{235}U. By M. Höjeberg and S. G. Malmskog 1969. 18 p. Sw. cr. 10:–.

372. E2 and M1 transition probabilities in odd mass Hg nuclei. By V. Berg, A Bäcklin, B. Fogelberg and S. G. Malmskog. 1969. 19 p. Sw. cr. 10:–

373. An experimental study of the accuracy of compensation in lithium drifted germanium detectors. By A. Lauber and B. Malmsten. 1969. 25 p. Sw. cr. 10:–.

374. Gamma radiation from fission fragments. By J. Higbie. 1969. 22 p. Sw. cr. 10:–.

375. Fast neutron elastic and inelastic scattering of vanadium. By B. Holmqvist, S. G. Johansson, G. Lodin and T. Wiedling. 1969. 48 p. Sw. cr. 10:–.

376. Experimental and theoretical dynamic study of the Ågesta nucler power station. By P. Å. Bliselius, H. Vollmer and F. Åkerhielm. 1969. 39 p Sw. cr. 10:–.

377. Studies of Redox equilibria at elevated temperatures 1. The estimation of equilibrium constants and standard potentials for aqueous systems up to 374°C. By D. Lewis. 1969. 47 p. Sw. cr. 10:–.

378. The whole body monitor HUGO II at Studsvik. Design and operation By L Devell, I. Nilsson and L. Venner. 1970. 26 p. Sw. cr. 10:–

279. ATOMSPHERIC DIFFUSION. Investigations at Studsvik and Ågesta 1960–1963. By L-E. Hæggblom, Ch. Gyllander and U. Widemo. 1969. 91 p Sw cr 10:–.

380. An expansion method to unfold proton recoil spectra. By J. Kockum. 1970. 20 p. Sw. cr. 10:–.

381. The 93.54 keV lever ^{91}Sr, and evidence for 3-neutron states above N=50. By S G. Malmskog and J. McDonald 1970. 24 p. Sw. cr. 10:–.

382. The low energy level structure of ^{191}Ir. By S. G. Malmskog, V. Berg, A. Bäcklin and G Hedin. 1970. 24 p Sw cr 10:–.

383. The drinking rate of fish in the Skagerack and the Baltic. By J. E. Larsson. 1970. 16 p. Sw. cr. 10:–.

384. Lattice dynamics of Nacl, KCl, RbCl and RbF. By G. Raunio and S. Rolandson. 1970. 26 p. Sw. cr. 10:–.

385. A neutron elastic scattering study of chromium, iron and nickel in the energy region 1.77 to 2.76 MeV. By B. Holmqvist, S. G. Johansson, G. Lodin, M Salama and T. Wiedling. 1970. 26 p. Sw. cr. 10:–.

386. The decay of bound isobaric analogue states in ^{28}Si and ^{32}Si using (d. nγ) reactions. By L. Nilsson, A Nilsson and I. Bergqvist. 1970. 34 p. Sw. cr. 10–.

387. Transition probabilities in ^{189}Os. By S. G. Malmskog, V. Berg and A. Bäcklin. 1970. 40 p. Sw. cr. 10:–.

388. Cross sections for high-energy gamma transition from MeV neutron capture in ^{208}Pb. By I. Bergqvist, B. Lundberg and L. Nilsson. 1970. 16 p. Sw. cr. 10:–.

389. High-speed, automatic radiochemical separations for activation analysis in the biological and medical research laboratory. By K. Samsahl. 1970. 18 p. Sw. cr. 10:–.

390. Use of fission product Ru-106 gamma activity as a method for estimating the relative number of fission events in U-235 and Pu-239 in low-enriched fuel elements. By R. S. Forsyth and W. H. Blackadder. 1970. 26 p. Sw. cr. 10:–.

391. Half-life measurements in ^{134}I. By V. Berg and A. Höglund. 1970. 16 p. Sw. cr. 10:–.

392. Measurement of the neutron spectra in FRO cores 5, 9 and PuB-5 using resonance sandwich detectors. By T. L. Andersson and M. N. Qazi. 1970. 30 p. Sw. cr. 10:–.

393. A gamma scanner using a Ge(Li) semi-conductor detector with the possibility of operation in anti-coincidence mode. By R. S. Forsyth and W. H. Blackadder. 1970. 22 p. Sw. cr. 10:–.

394. A study of the 190 keV transition in ^{141}La. By B. Berg, A. Höglund and B. Fogelberg. 1970. 22 p. Sw. cr. 10:–.

395. Magnetoacoustic waves and instabilities in a Hall-effect-dominiated plasma. By S. Palmgren. 1970. 20 p. Sw. cr. 10:–.

396. A new boron analysis method. By J. Weitman, N. Dåverhög and S. Farvolden. 1970 26 p. Sw. cr. 10:–.

397. Progress report 1969. Nuclear chemistry. 1970. 39 p. Sw. cr. 10:–.

398. Prompt gamma radiation from fragments in the thermal fission of ^{235}U. By H. Albinsson and L. Lindow. 1970. 48 p. Sw. cr. 10:–.

399. Analysis of pulsed source experiments performed in copper-reflected fast assemblies. By J. Kockum. 1970. 32 p. Sw. cr. 10:–.

400. Table of half-lives for excited nuclear levels. By S. G. Malmskog. 1970. 33 p. Sw. cr. 10:–.

401. Needle type solid state detectors for in vivo measurement of tracer activity. By A. Lauber, M. Wolgast. 1970. 43 p. Sw. cr. 10:–.

402. Application of pseudo-random signals to the Ågesta nuclear power station. By P-Å. Bliselius. 1970. 30 p. Sw. cr. 10:–.

403. Studies of redox equilibria at elevated temperatures 2. An automatic divided-function autoclave and cell with flowing liquid junction for electrochemical measurements on aqueous systems. By. K. Johnsson, D. Lewis and M. de Pourbaix. 1970. 38 p. Sw. cr. 10:–.

404. Reduction of noise in closed loop servo systems. By K. Nygaard. 1970. 23 p. Sw. cr. 10:–.

405. Spectral parameters in water-moderated lattices. A survey of experimental data with the aid of two-group formulae. By E. K. Sokolowski. 1970. 22 p. Sw. cr. 10:–.

406. The decay of optically thick helium plasmas, taking into account ionizing collisions between metastable atoms or molecules. By J. Stevefelt. 1970. 18 p. Sw. cr. 10:–.

407. Zooplankton from Lake Magelungen, Central Sweden 1960-63. By E. Almquist. 1970. 62 p. Sw. cr. 10:–.

408. A method for calculating the washout of elemental iodine by water sprays. By E Bachofner and R. Hesböl. 1970. 24 p. Sw. cr. 10:–.

409. X-ray powder diffraction with Guinier–Hägg focusing cameras. By A. Brown. 1970. 102 p. Sw. cr 10:–.

410. General physic section Progress report. Fiscal year 1969/70. By J. Braun. 1970. 92 p. Sw cr. 10:–.

411. In-pile determination of the thermal conductivity of UO_2 in the range 500–2 500 degrees centigrade. By J-Å Gyllander. 1971. 70 p. Sw. cr. 10:–.

412. A study of the ring test for determination of transverse ductility of fuel element canning. By G. Anevi and G. Östberg. 1971. 17 p. Sw. cr. 15:–.

413. Pulse radiolysis of Aqueous Solutions of aniline and substituted anilines. By H. C. Christensen. 1971. 40 p. Sw. cr. 15:–.

414. Radiolysis of aqueous toluene solutions. By H. C. Christensen and R. Gustafson. 1971. 20 p. Sw. cr. 15:–.

415. The influence of powder characteristics on process and product parameters in UO_2 pelletization. By U. Runfors. 1971. 32 p. Sw. cr. 15:–.

416. Quantitative assay of Pu239 and Pu240 by neutron transmission measurements. By E. Johansson. 1971. 26 p. Sw. cr 15:–.

417. Yield of prompt gamma radiation in slow-neutron induced fission of ^{235}U as a function of the total fragment kinetic energy. By H. Albinsson. 1971. 38 p. Sw. cr. 15:–.

418. Measurements of the spectral light emission from decaying high pressure helium plasmas. By J. Stevefelt and J. Johansson. 1971. 48 p. Sw. cr. 15:–.

419. Progress report 1970. Nuclear chemistry. 1971. 32 p. Sw. cr. 15:–.

420. Energies and yields of prompt gamma rays from fragments in slow-neutron induced fission of ^{235}U. By H. Albinsson. 1971. 56 p. Sw. cr. 15:–.

421. Decay curves and half-lives of gamma-emitting states from a study of prompt fission gamma radiation. By H. Albinsson. 1971. 28 p. Sw. cr. 15:–.

422. Adjustment of neutron cross section data by a least square fit of calculated quantities to experimental results. Part 1. Theory. By H. Häggblom. 1971. 28 p. Sw. cr. 15:–.

423. Personnel dosimetry at AB Atomenergi during 1969. By J. Carlsson and T. Wahlberg. 1971. 10 p. Sw. cr. 15:–.

424. Some elements of equilibrium diagrams for systems of iron with water above 100°C and with simple chloride, carbonate and sulfate melts. By D. Lewis. 1971. 40 p. Sw. cr. 15:–.

425. A study of material buckling in uranium-loaded assemblies of the fast reactor FR0. By R. Håkansson and L. I. Tirén. 1971. 32 p. Sw. cr. 15:–.

426. Dislocation line tensions in the noble metals, the alkali metals and β-Brass. By B. Pettersson and K. Malén. 1971. 14 p. Sw. cr. 15:–.

427. Studies of fine structure in the flux distribution due to the heterogeneity in some FR0 cores. By T. L. Andersson and H. Häggblom. 1971. 32 p Sw. cr. 15:–.

428. Integral measurement of fission-product reactivity worths in some fast reactor spectra. By T. L. Andersson. 1971. 36 p. Sw. cr. 15:–.

429. Neutron energy spectra from neutron induced fission of ^{235}U at 0.95 MeV and of ^{238}U at 1.35 and 2.02 MeV. By E. Almén, B. Holmqvist and T. Wiedling. 1971. 16 p. Sw. cr. 15:–.

430. Optical model analyses of experimental fast neutron elastic scattering data. By B. Holmqvist and T. Wiedling. 1971. 238 p. Sw. cr. 20:–.

431. Theoretical studies of aqueous systems above 25°C. 1. Fundamental concepts for equilibrium diagrams and some general features of the water system. By Derek Lewis. 1971. 27 p. Sw. cr. 15:–.

432. Theoretical studies of aqueous systems above 25°C . 2. The iron – water system. By Derek Lewis. 1971. 41 p. Sw. cr. 15:–.

433. A detector for (n,γ) cross section measurements. By J Hellström and S. Beshai. 1971. 22 p. Sw. cr. 15:–.

434. Influence of elastic anisotropy on extended dislocation nodes. By B. Pettersson. 1971. 27 p. Sw. cr. 15:–.

List of published AES-reports (In Swedish)

1. Analysis by means of gamma spectrometry. By D. Brune. 1961. 10 p. Sw. cr. 6:–.
2. Irradiation changes and neutron atmosphere in reactor pressure vessels-some points of view. By M. Grounes. 1962. 33 p. Sw. cr. 6:–.
3. Study of the elongation limit in mild steel. By G. Östberg and R. Attermo. 1963. 17 p. Sw. cr. 6:–.
4. Technical purchasing in the reactor field. By Erik Jonson. 1963. 64 p. Sw. cr. 8:–.
5. Ågesta nuclear power station. Summary of technical data, descriptions, etc. for the reactor. By B. Lilliehöök. 1964. 336 p. Sw. cr. 15:–.
6. Atom Day 1965. Summary of lectures and discussions. By S. Sandström. 1966. 321 p. Sw. cr. 15:–.
7. Building materials containing radium considered from the radiation protection point of view. By Stig O. W. Bergström and Tor Wahlberg. 1967. 26 p. Sw. cr. 10:–.
8. Uranium market. 1971. 30 p. Sw. cr. 15:–.

Additional copies available from tha Library of AB Atomenergi, Fack, S-611 01 Nyköping 1, Sweden.

EOS-tryckerierna, Stockholm 1971